Int. J. Electrochem. Sci., 11 **(2016)** 1512 - 1529

International Journal of ELECTROCHEMICAL SCIENCE
www.electrochemsci.org

Oxidation Characteristic and Machining Performance of Reaction-Sintered Silicon Carbide Ceramic in Anodically Oxidation-Assisted Polishing

Guoliang Jiang[1], *Xinmin Shen*[1,*], *Jian Tang*[1], *Xiaonan Zhang*[1], *Xiangpo Zhang*[1], *Kazuya Yamamura*[2,*]

[1]College of Field Engineering, PLA University of Science and Technology, Jiangsu 210007, China.
[2]Graduate School of Engineering, Osaka University, Osaka 565-0871, Japan.
[*]E-mail: shenxmjfjlgdx2014@163.com ; yamamura@upst.eng.osaka-u.ac.jp

Received: 11 November 2015 / *Accepted:* 10 December 2015 / *Published:* 1 January 2016

A novel method for machining reaction-sintered silicon carbide (RS-SiC) ceramic using anodically oxidation-assisted polishing is proposed. Through anodic oxidation of RS-SiC, hardness of the oxidized sample can be reduced, and the soft oxide layer is easy to be machined with the assistance of abrasive polishing. In this way, fine surface quality and high material removal rate can be obtained in machining RS-SiC. The influences of process conditions on the oxide morphology, oxidation rate, and surface roughness have been qualitative investigated with scanning electron microscope (SEM) and quantitative analyzed with scanning white light interferometry (SWLI). The results show that anodic oxidation of RS-SiC by phosphoric acid (H_3PO_4) under the constant potential can obtain soft oxide and smooth morphology; abrasive polishing of oxide layer can obtain smooth surface with roughness rms 8.520nm. Relationship between oxidation depth and its influencing factors can be theoretical analyzed based on the oxidation mechanism, and the oxidation depth can be calculated by hydrofluoric acid (HF) etching of the oxidized sample. It can be concluded that the anodically oxidation-assisted polishing, which includes the anodic oxidation of RS-SiC by H_3PO_4 and abrasive polishing of oxide layer by ceria slurry, can be treated as a practical method to machine RS-SiC.

Keywords: anodically oxidation-assisted polishing; reaction-sintered silicon carbide; phosphoric acid; oxidation characteristic; machining performance.

1. INTRODUCTION

Electrochemical method is gradually introduced into ultraprecision machining fields, especially for some difficult-to-machine (DTM) materials, for example, reaction-sintered silicon carbide (RS-SiC). RS-SiC is a promising and excellent material for various applications, such as the optical mirror devices in space telescope systems [1], corrosion-resistant composites in chemical plants [2], mold

components in aspheric lens formation apparatus [3], and the radionresistant parts in nuclear fusion equipment [4]. RS-SiC has excellent physical, electrical, mechanical, and chemical properties, such as the advantages of a high radiation resistance, low thermal expansion coefficient, high thermal conductivity, good size stability, high specific stiffness, and a low manufacturing cost [5-7]. Thus, the fabrication and machining of RS-SiC is the research focus in the fields of ceramics and optics [8-10].

However, the high hardness and chemical inertness makes RS-SiC a representative DTM material [11], which limits the efficient techniques for the rapid figuring of RS-SiC substrate. Meanwhile, the fabrication process of RS-SiC generates SiC and Si domains as the major components in the substrate [12-14], which indicates that the fine finishing of RS-SiC is difficult to obtain an ultrasmooth surface. Thus, few of present techniques for machining RS-SiC can achieve a high material removal rate (MRR) in the rough figuring process and yield an ultrasmooth surface in the fine finishing process [12-14].

Fortunately, both the oxides of SiC and Si are silica (SiO_2), and the hardness of the oxide is much lower than that of the initial RS-SiC substrate. Therefore, a feasible and promising machining method, named oxidation-assisted polishing, had been developed to improve the MRR and the surface quality in machining RS-SiC [15-17]. By the thermal oxidation, plasma oxidation, or anodic oxidation, soft oxide layers can be obtained on the RS-SiC substrates, which is propitious to obtain high MRR and to yield ultrasmooth surface by combination with the assistance of abrasive polishing [16].

Anodic oxidation is an effective method for the oxidation-assisted polishing of RS-SiC relative to thermal oxidation and plasma oxidation, because the rate in anodic oxidation of RS-SiC is thousand times higher than that in plasma oxidation or that in thermal oxidation [16]. The main factors in anodic oxidation of RS-SiC are electrolyte, potential, and oxidation time. Phosphoric acid (H_3PO_4) is a classic electrolyte that has been widely used in the electrochemical process [18], which is chose to oxidize RS-SiC substrate in this study. In the anodic oxidation process, the common power supply has two modes: high-frequency-square-wave (HFSW) potential and constant potential. These two modes are both examined in this study. By scanning electron microscopy (SEM) observation and scanning white light interferometry (SWLI) measurement, the oxidation characteristic and machining performance of RS-SiC samples in different process conditions are investigated and analyzed. In order to further analyze the anodic oxidation process, the relationship between oxidation depth and its influencing factors is theoretically analyzed based on the anodic oxidation mechanism, and the oxidation depth is calculated by hydrofluoric acid (HF) etching of the oxidized sample to verify the theoretical analysis.

2. EXPERIMENTAL SETUP

The system for anodic oxidation of RS-SiC under the HFSW potential is shown in Fig. 1(a). The square wave is generated from the digital function generator (DFG). The HFSW potential is exported from the high speed bi-polar power supply. The digital storage oscilloscope (DSO) is used to monitor the status of oxidation circuit. The electrolyte (H_3PO_4) fills the container, which forms the oxidation circuit by combination with anode (RS-SiC) and cathode (Platinum, Pt). Electrical current is generated between the anode and cathode under the HFSW potential. Thus, oxide is formed on the RS-

SiC sample at the region that contacts the electrolyte. Meanwhile, the system for anodic oxidation of RS-SiC under the constant potential is shown in Fig. 1(b). The constant potential is exported from the potentiostat. The oxidation current is incessantly recorded by the sampling software in the computer. The reference electrode (Ag/AgCl) is used to keep the potential constant by feedback control. Similar with the anodic oxidation of RS-SiC under the HFSW potential, in the constant potential mode, the electrical current is generated between the anode and cathode, and the oxide can be formed at the region of RS-SiC sample that contacts the electrolyte. The summarized anodic oxidation parameters are shown in Table 1. The major influencing factors in the anodic oxidation process are potential mode, electrolyte and its concentration, and oxidation time. Therefore, in order to make a fair comparison of the two potential modes, the equivalent oxidation voltages in the two modes are both set to 9.8V. The oxidation time is also set to be the same (30min). Distances between the anode and cathode, oxidized areas of the RS-SiC sample, radiuses of the container, and sizes of the cathode are also the same in the two modes.

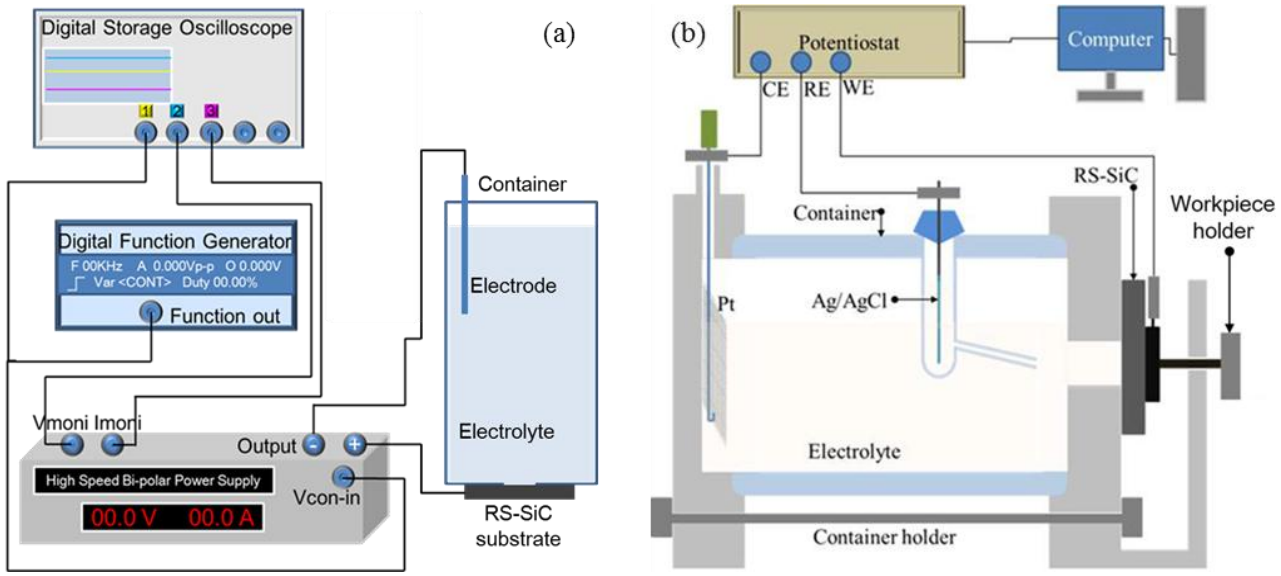

Figure 1. Schematic diagrams of the anodic oxidation systems. (a) in the HFSW potential mode. (b) in the constant potential mode.

Table 1. The summarized anodic oxidation parameters.

Parameters	In the HFSW potential mode	In the constant potential mode
Oxidation voltage	19.6V (square wave), 20KHz, 50%	9.8V (constant)
Cathode	Platinum (Pt)	Platinum (Pt)
Anode	RS-SiC sample	RS-SiC sample
Electrolyte	H_3PO_4	H_3PO_4
Concentration	10wt%	10wt%
Reference electrode	-	Ag/AgCl
Oxidation time	30min	30min

In order to investigate the machining performance of the oxide layers obtained in the two potential modes, the oxidized RS-SiC samples are polished by ceria (CeO_2) slurry, and schematic diagram of the polishing system is shown in Fig. 2. The reason for the application of abrasive polishing method is that it is easy to obtain high MRR and yield ultrasmooth surface simultaneously in polishing of silica (SiO_2) by CeO_2 in chemical mechanical polishing (CMP) [19, 20]. The oxidized RS-SiC sample is fixed on the stage, while the oxidized surface contacts the slurry. The polishing pad is immersed into the slurry, and the oxidized RS-SiC sample is abraded by the polishing pad. The load can be adjusted by changing weights on the load plate. The summarized abrasive polishing parameters are shown in Table 2. After abrasive polishing, the RS-SiC sample is detected by SWLI and SEM to evaluate the surface qualities.

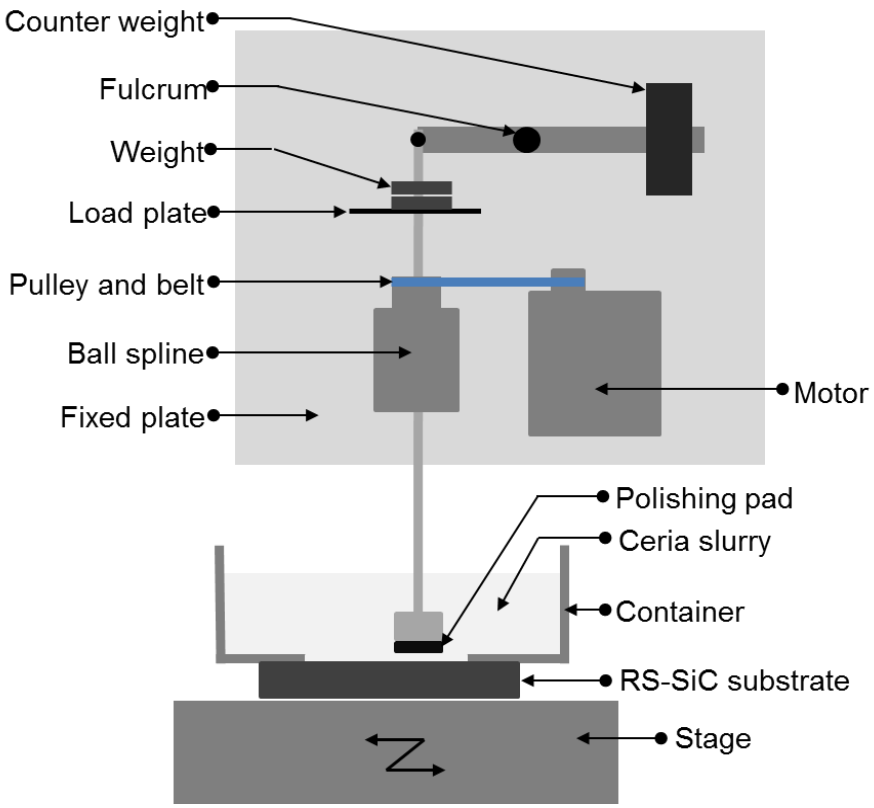

Figure 2. Schematic diagram of the abrasive polishing system.

Table 2. The summarized abrasive polishing parameters.

Parameters	Values
Specimen and its size	Oxidized RS-SiC, 15mm × 15mm
Abrasive and its size	Ceria, ϕ190nm
Slurry concentration	0.1wt%
Load and downward pressure	20g, 2.495kPa
Rotation speed and scanning speed	800rpm, 200mm/min
Polishing pad and its size	K0017 (FILWEL Co. Ltd.), ϕ10mm

3. RESULTS

3.1 Oxidation characteristic in the HFSW potential mode

After anodic oxidation under the HFSW potential, the oxidized RS-SiC sample is investigated by SEM observation, and the comparisons of surface morphologies before and after anodic oxidation at the same position are shown in Fig. 3. The initial SiC grains and Si grains in the RS-SiC sample are identified by the scanning electron microscope / energy dispersive X-ray spectroscopy (SEM-EDX), and the representative SiC grains and Si grains are marked in Fig. 3(a). Through comparing the surface morphologies before anodic oxidation in Fig. 3(a) and those after anodic oxidation in Fig. 3(b), it can be found that the oxides generated from original SiC grains form many protuberances, and there are many ditches on the oxide. Meanwhile, oxides generated from original Si grains have a relatively smooth surface, and there are few cracks or ditches on the oxidized grains.

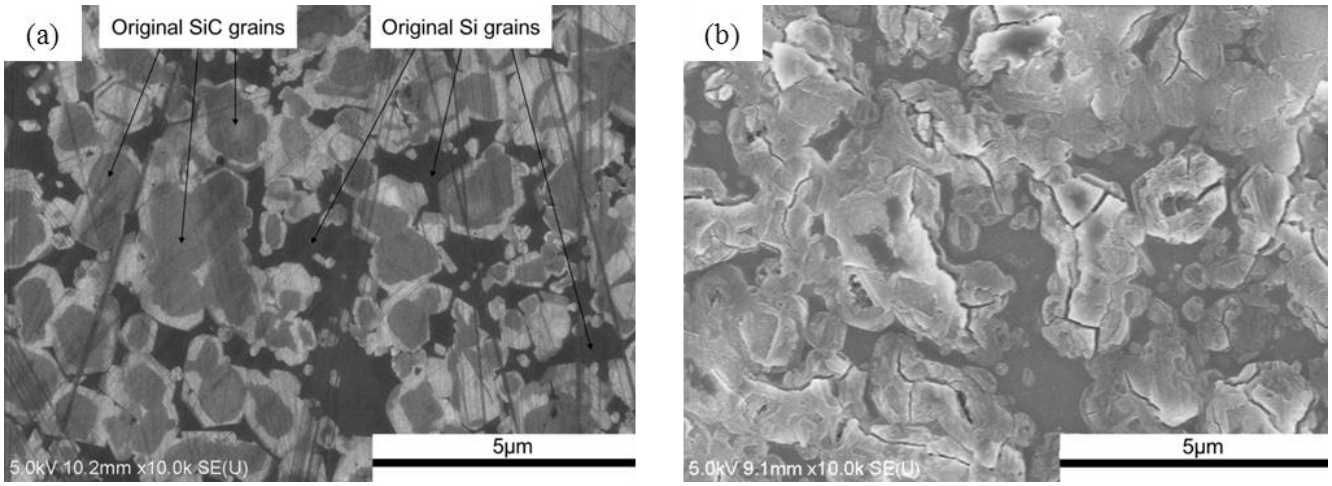

Figure 3. Comparisons of the surface morphologies before and after anodic oxidation at the same position in the HFSW potential mode. (a) the original RS-SiC surface. (b) the oxidized surface.

From the oxidation mechanism, we hypothesize that the oxidation characters in anodic oxidation of RS-SiC under the HFSW potential are caused by the uneven distribution of volume expansion force. The oxidation of SiC/Si to SiO_2 is a volume expansion process, so the expansion forces are inevitably generated. The magnitude and direction of the force is determined by the distribution of the oxidation current and the orientation of the grain. According to the knowledge of crystallology, it can be found that most of the oxidation currents focus at the surface of the SiC grains. Therefore, the oxidation rates of SiC grains are higher than those of Si grains, and the central area has a lower oxidation rate than the boundary region in a certain SiC grain. What's more, the expansion forces cause that the oxides of initial SiC/Si grains extrude each other, so the protuberances are formed by the extrusion force, and the cracks are formed by the expansion force generated from the oxidation of subsurface grains. Since different SiC grains in the RS-SiC sample have different crystal lattice parameters, directions of the expansion forces are desultorily. Thus, protuberance and crack are

introduced on the oxides generated from SiC grains. In contrast, the Si grains in the RS-SiC sample are amorphous silicon, which have no difference in the lattice parameters. Thus, the oxides generated from Si grains have smooth surfaces.

In order to further investigate the oxidation characters, details of subsurface morphologies obtained by SEM observation with high magnification are obtained, as shown in Fig. 4. From Fig. 4(a) it can be found that there are many cracks at the boundaries between the SiC grains and Si grains, which are generated by differences of the oxidation rate. There are cracks on the oxides of initial SiC grains, as shown in Fig. 4(b), and width of some cracks is over 200nm. These are unpropitious to yield smooth surface with the abrasive polishing. Furthermore, some cracks penetrate into the inside of RS-SiC, as shown in Fig. 4(a). They are difficult to remove entirely. Therefore, anodic oxidation of RS-SiC in the HFSW potential mode is difficult to obtain smooth surface with the assistance of abrasive polishing.

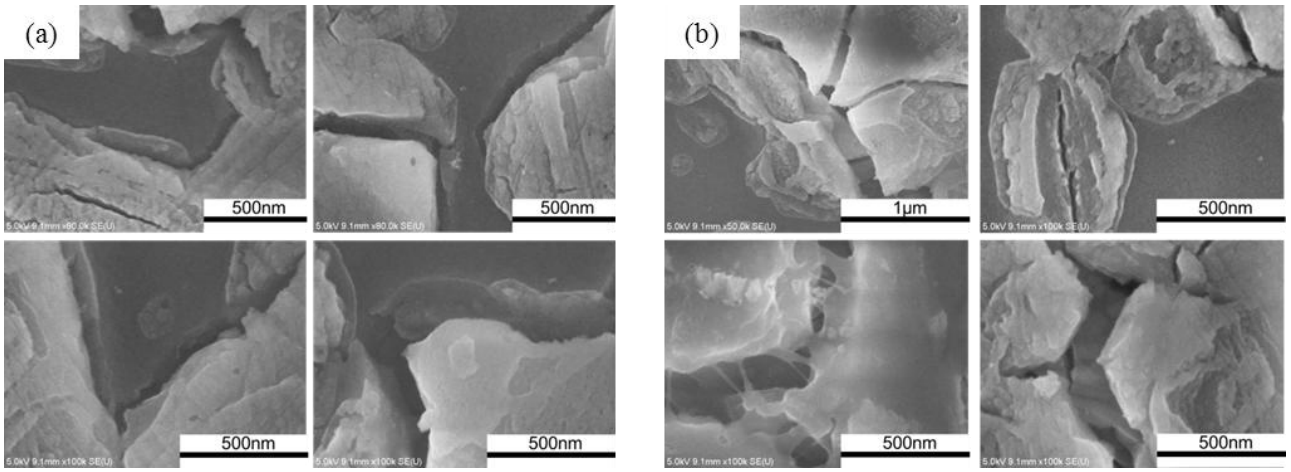

Figure 4. Details of subsurface morphologies in anodic oxidation under the HFSW potential. (a) morphologies of the boundary region. (b) morphologies of the oxide generated from initial SiC grain.

3.2 Oxidation characteristic in the constant potential mode

Meanwhile, the RS-SiC sample oxidized by H_3PO_4 under the constant potential is also investigated by SEM observation, and the comparisons of surface morphologies before and after anodic oxidation at the same position are shown in Fig. 5. There are some similar oxidation characters between the RS-SiC samples oxidized under the constant potential in Fig. 5(b) and that oxidized under the HFSW potential in Fig. 3(b). For example, oxidation rates of SiC grains are higher than those of Si grains; central area has a lower oxidation rate relative to the boundary region in a certain SiC grain; there are obvious cracks on the oxides generated from initial SiC grains; oxides of the Si grains have relatively smooth surfaces. These are common characters in anodic oxidation of RS-SiC [16], which are also the most obvious characters to identify anodic oxidation from plasma oxidation and thermal oxidation.

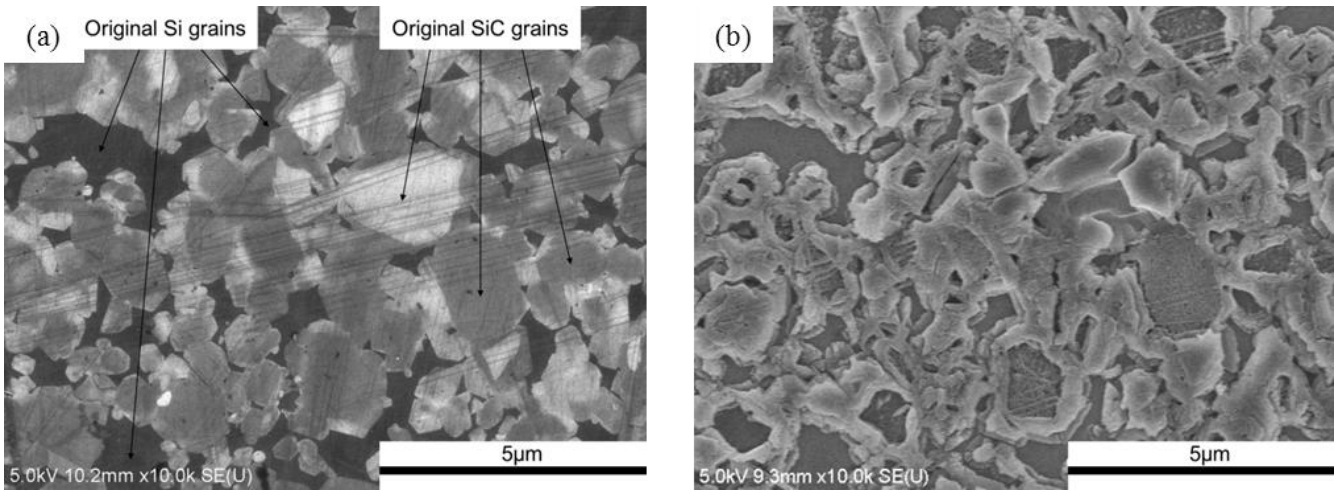

Figure 5. Comparisons of the surface morphologies before and after anodic oxidation at the same position in the constant potential mode. (a) the original RS-SiC surface. (b) the oxidized surface.

However, it can be found that there are some obvious differences between the surface morphologies in Fig. 3(b) and those in Fig. 5(b). Sizes of the oxides obtained under the constant potential are larger than those obtained under the HFSW potential, and the cracks in Fig. 5(b) are thinner than those in Fig. 3(b). What's more, contrasts of the oxide morphologies generated from initial SiC grains and Si grains in Fig. 5(b) are clearer than those in Fig. 3(b). The common oxidation characters in anodic oxidation of RS-SiC are more remarkable in Fig. 5(b). The differences of oxidation characters are generated by the differences of potential modes. We suppose that the reasons for those are the differences of modality and distribution of the electricity in the oxidation process. In the anodic oxidation of RS-SiC under the HFSW potential, the electrical current with a high frequency causes a drastic and indefinite oxidation reaction, and the volume expansion forces generated from the oxidation process destroy the oxidized RS-SiC surface. In contrast, in the anodic oxidation of RS-SiC under the constant potential, chemical reaction in the oxidation process is gently and determinate. Thus, the volume expansion forces in the anodic oxidation of RS-SiC under the constant potential are steady and invariable, which can form oxidized surfaces with relatively smooth morphologies. Therefore, anodic oxidation of RS-SiC under the constant potential is possible to obtain smooth surface with the assistance of abrasive polishing.

In order to further investigate the oxidation characters, details of subsurface morphologies in the anodic oxidation of RS-SiC under the constant potential are obtained, as shown in Fig. 6. From Fig. 6(a), it can be found that central region of the oxide generated from initial SiC grain has many small projections, which is similar with the morphology in anodic oxidation of single crystal SiC [21]. Meanwhile, there are fewer cracks on the oxidized surface shown in Fig. 6(a) relative to that shown in Fig. 4(b). From Fig. 6(b) it can be observed that the cracks among the initial SiC grains and Si grains in the constant potential mode are on the surface, which are different from those shown in Fig. 4(a). In the HFSW potential mode, the cracks penetrate into the oxidized RS-SiC sample, which is very difficult to remove with the assistance of abrasive polishing.

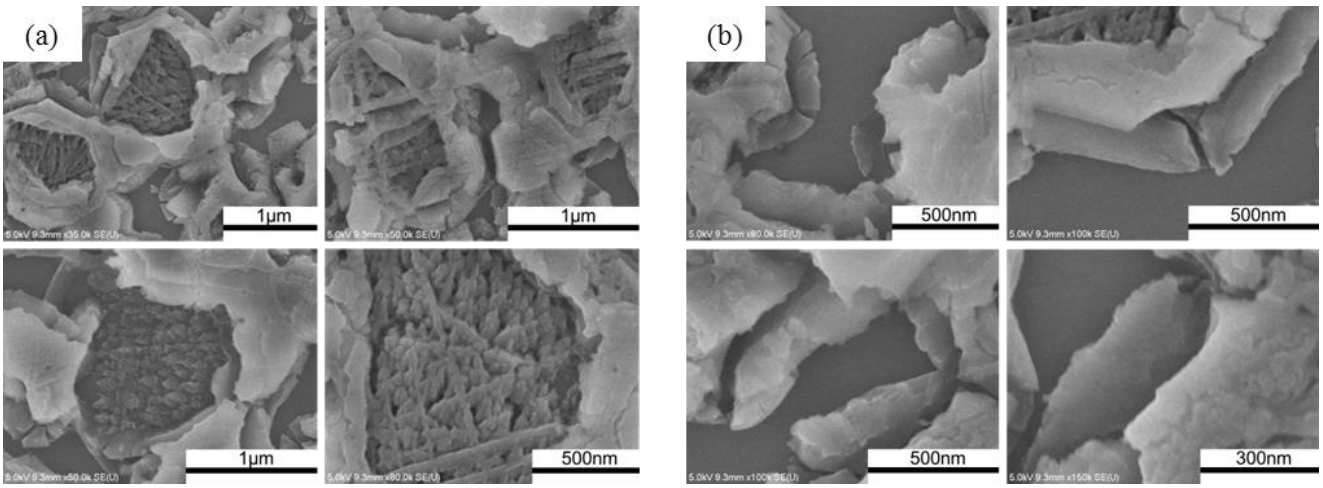

Figure 6. Details of subsurface morphologies in anodic oxidation under the constant potential. (a) morphologies of the oxide generated from initial SiC grain. (b) morphologies of the boundary region.

Hardness of the oxide is obviously lower than that of the initial RS-SiC samples, and the projections and cracks on the soft oxide increase the contact areas with the CeO_2 particles in the abrasive polishing process. These characters make it easier to obtain high MRR and smooth surface in the anodically oxidation-assisted polishing process relative to the directly machining of the RS-SiC substrate.

From the qualitative analysis of the oxidation characters of the two potential modes, it can be found that the anodic oxidation of RS-SiC under the constant potential can form a relatively smooth surface, which is propitious to obtain better surface quality with the assistant of abrasive polishing.

3.3 Quantitative analysis of surface qualities in the two potential modes

In order to further quantitative analyze the surface qualities of the anodic oxidized RS-SiC samples, the detections by SWLI are conducted, and the results are shown in Fig. 7. The surface roughness rms of the oxidized RS-SiC sample under the HFSW potential is 196.321nm, and that obtained under the constant potential is 148.095nm. After anodic oxidation, the surface qualities are destroyed, as shown in Fig. 7(a) and Fig. 7(c), because there are many protuberances and cracks on the oxidized surfaces. The oxidized surface obtained under the constant potential is slightly better than that obtained under the HFSW potential. Through comparing of the cross-sectional lines of two oxidized surfaces in Fig. 7(b) and Fig. 7(d), it can be observed that the quantities and sizes of the protuberances and cracks on the oxidized surface obtained under the HFSW potential are larger than those obtained under the constant potential. It can also be judged from the peak-to-valley (PV) value of the oxidized surfaces. PV of the oxidized surface obtained under HFSW potential is 3184.945nm, and that obtained under the constant potential is 2663.192nm. The results of quantitative analysis are consistent with those in the qualitative investigation, which further approves that anodic oxidation of RS-SiC by H_3PO_4 under the constant potential is propitious to obtain better surface quality through the

combination with abrasive polishing. The further research focuses on the anodic oxidation of RS-SiC under the constant potential.

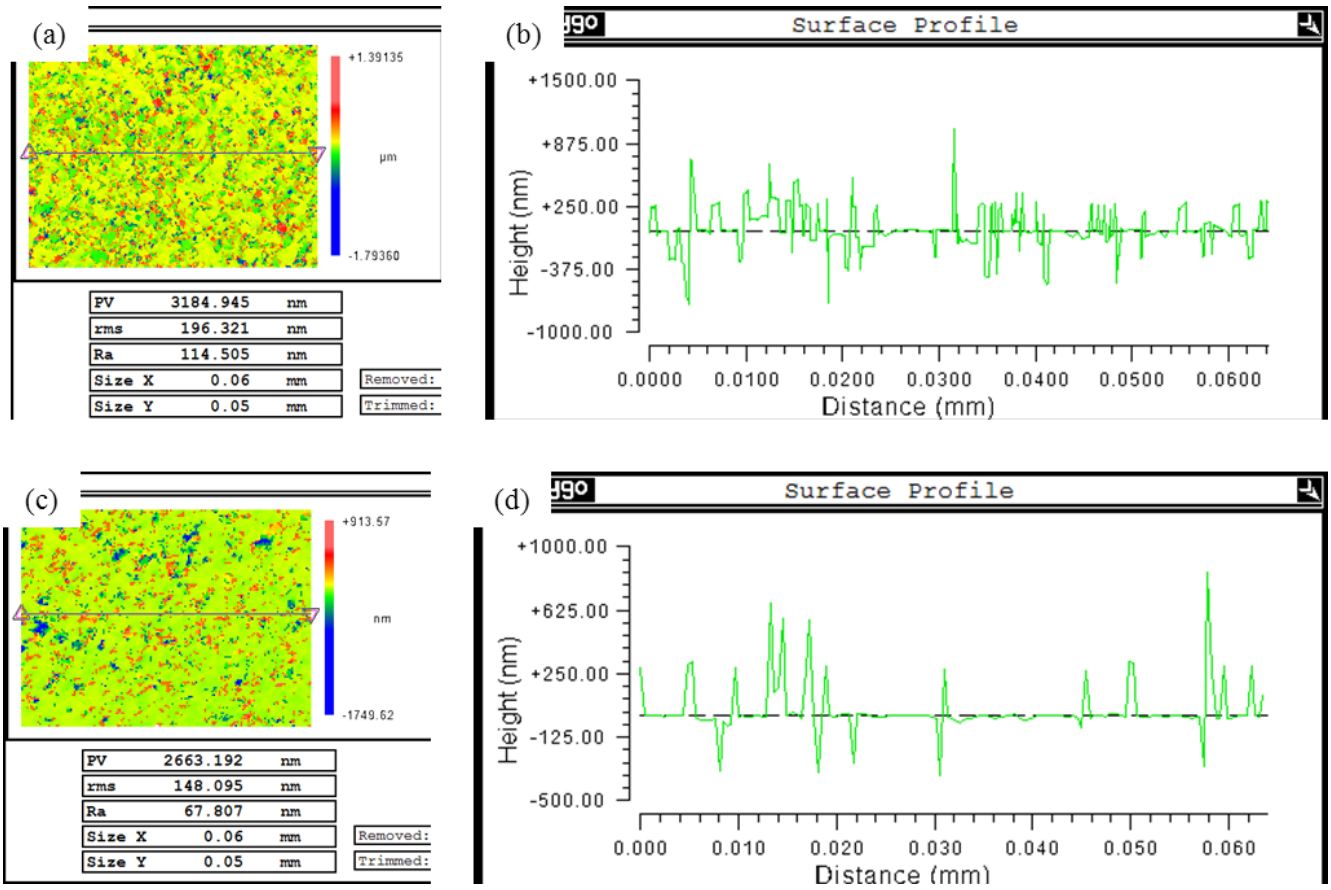

Figure 7. Quantitative analysis of surface qualities of the oxidized RS-SiC samples in the two potential modes. (a) anodic oxidation under the HFSW potential. (b) profile of the cross-sectional line in (a). (c) anodic oxidation under the constant potential. (d) profile of the cross-sectional line in (c).

3.4 Validation of machining performance of the oxide layers

The oxidized RS-SiC samples obtained in the two potential modes are further machined by the abrasive polishing system, as shown in Fig. 2. The aim is to investigate the machining performance of the oxide layers. The polished RS-SiC samples are detected by SWLI, and the results are shown in Fig. 8. After polishing of the oxidized RS-SiC obtained under the HFSW potential, the surface roughness rms is 52.771nm, and after polishing of that obtained under the constant potential is 8.520nm. This is consistent with the results of analysis on the oxidation characters and oxide morphologies in the two potential modes. Thus, the anodically oxidation-assisted polishing, which includes anodic oxidation of RS-SiC by H_3PO_4 under the constant potential and abrasive polishing of oxide layer by CeO_2 slurry, can be considered as a practical method for the efficient machining of RS-SiC substrates.

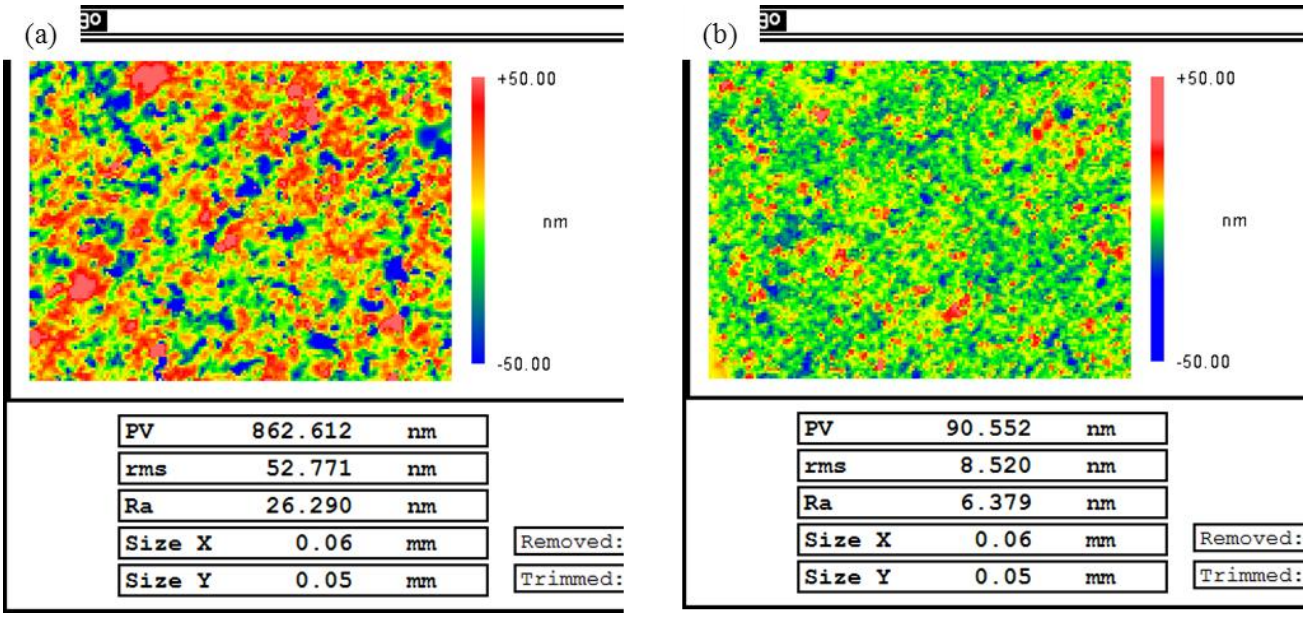

Figure 8. Evaluation of machining performance of the oxide layers in the two potential modes. (a) after polishing of the oxidized RS-SiC sample obtained in the HFSW potential mode. (b) after polishing of the oxidized RS-SiC sample obtained in the constant potential mode.

4. DISCUSSION

4.1 Investigation of the oxidation process

From the knowledge in the electrochemistry, it can be found that the anodic oxidation of RS-SiC sample is realized by oxidation potential of the electric charge [18]. The electric charge is driven by the voltage, which forms the oxidation current. The SiC grains and Si grains in the RS-SiC sample, which contact the electrolyte, are oxidized by the electric charge. At the anode side, formulas of the chemical reactions for the oxidation of SiC grains and Si grains are shown in Eq. 1 and Eq. 2, respectively.

$$SiC + 4p^{+} + 2H_2O \rightarrow SiO_2 + 4H^{+} + C \quad (1)$$

$$Si + 4p^{+} + 2H_2O \rightarrow SiO_2 + 4H^{+} \quad (2)$$

Meanwhile, at the cathode side, the water (H_2O) molecule around the cathode receives the electron driven by the voltage, and the formula of the chemical reaction is shown in Eq. 3.

$$H_2O + 2e^{-} \rightarrow H_2 \uparrow + 4OH^{-} \quad (3)$$

At the same time, in the electrolyte, the H_2O molecule receives the electric charge driven by the voltage, and the oxygen (O_2) is produced. The corresponding chemical reaction is shown in Eq. 4.

$$2H_2O + 4p^{+} \rightarrow O_2 \uparrow + 4H^{+} \quad (4)$$

Simultaneously, H_2O molecule is composed by the combination of hydroxyl (H^{+}) and hydrogen ion (OH^{-}) in the oxidation process, and the formula of the chemical reaction is shown in Eq. 5.

$$H^{+} + OH^{-} \rightarrow H_2O \quad (5)$$

Therefore, the summarized formulas for the anodic oxidation of SiC grains and Si grains in RS-SiC substrate can be concluded, as shown in Eq. 6 and Eq. 7, respectively.

$$SiC + 4H_2O \xrightarrow{8p^+/8e^-} SiO_2 + C + 2H_2\uparrow + O_2\uparrow \quad (6)$$

$$Si + 4H_2O \xrightarrow{8p^+/8e^-} SiO_2 + 2H_2\uparrow + O_2\uparrow \quad (7)$$

4.2 Derivation of the theoretical oxidation depth

From the summarized formulas in Eq. 6 and Eq. 7, it can be found that it needs 8 positive/negative charges to oxidize 1 SiC/Si molecule to 1 SiO_2 molecule. Therefore, the volume of the formed oxide is in positive proportional to the summation of the passed charges from the anode to the cathode. Since not all the passed charges participate in the oxidation process, the utilization coefficient is assumed as μ. Based on the principle of equilibrium in chemical reaction, the following equation can be obtained.

$$\mu Q : \frac{\pi r^2 dD}{M} = 8:1 \quad (8)$$

Where μ, Q, r, d, D, M are the utilization coefficient of the electric charge, summation of the passed charges, radius of the oxidized spot (the oxidized area is a column), oxidation depth, density of the oxide (SiO_2), and Molar mass of SiO_2, respectively.

According to the definition of current, the summation of the passed charges Q can be calculated by the integration of the oxidation current I. The relationship between Q and I is shown in Eq. 9.

$$Q = \int_0^t I dt \quad (9)$$

According to the Ohm's law, the current is proportional to the voltage V, and is also proportional to the concentration of free ions f in the electrolyte. Supposing the proportional coefficient is k, and the expression of the current is $i(t)$. Therefore, the oxidation current I can be calculated by the Eq. 10.

$$I = kVf \cdot i(t) \quad (10)$$

The concentration of free ions f is determined by the concentration and electrolysis of the electrolyte. The electrolysis processes of H_3PO_4 are shown in Eq. 11.

$$H_3PO_4 \rightarrow H^+ + H_2PO_4^- \quad pK_{a1} = 2.15$$
$$H_2PO_4^- \rightarrow H^+ + HPO_4^{2-} \quad pK_{a2} = 7.20 \quad (11)$$
$$HPO_4^{2-} \rightarrow H^+ + PO_4^{3-} \quad pK_{a3} = 12.37$$

It includes H^+, $H_2PO_4^-$, HPO_4^{2-}, PO_4^{3-} and few OH^- ions in the electrolyte, as shown in Fig. 9, and the concentration of the free ions f is the summation of them. Supposing the concentration of the electrolyte is c, and the concentrations of $H_2PO_4^-$, HPO_4^{2-}, PO_4^{3-} can be calculated as $c^{\frac{1}{2}} \cdot pK_{a1}^{\frac{1}{2}}$, $c^{\frac{1}{4}} \cdot pK_{a1}^{\frac{1}{4}} \cdot pK_{a2}^{\frac{1}{2}}$, $c^{\frac{1}{8}} \cdot pK_{a1}^{\frac{1}{8}} \cdot pK_{a2}^{\frac{1}{4}} \cdot pK_{a2}^{\frac{1}{2}}$, respectively. From the Eq. 11 it can be found that the concentration of the H^+ ions is the summation of them three. Meanwhile, the concentration of the OH^- ions is 10^{-14} divided by the concentration of the H^+ ions. Since the concentrations of the HPO_4^{2-}, PO_4^{3-} and OH^- ions are very low in the applied electrolyte, the concentration of free ions f is mostly consisted of the $H_2PO_4^-$ and H^+ ions. Thus, f can be calculated by the Eq. 12.

$$f = 2c^{\frac{1}{2}} \cdot pK_{a1}^{\frac{1}{2}} \quad (12)$$

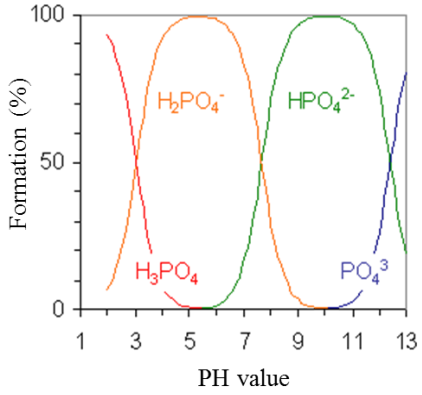

Figure 9. The formations of free ions in the H_3PO_4 eleotrolyte.

The detected oxidation current with the increasing of oxidation time under the constant potential is shown Fig. 10. By data fitting it can be found that the curve of the current *i(t)* is power function, and the power coefficient is -0.75. Thus, the oxidation current can be calculated with the following Eq. 13.

$$I = k \cdot V \cdot f \cdot t^{-0.75} \quad (13)$$

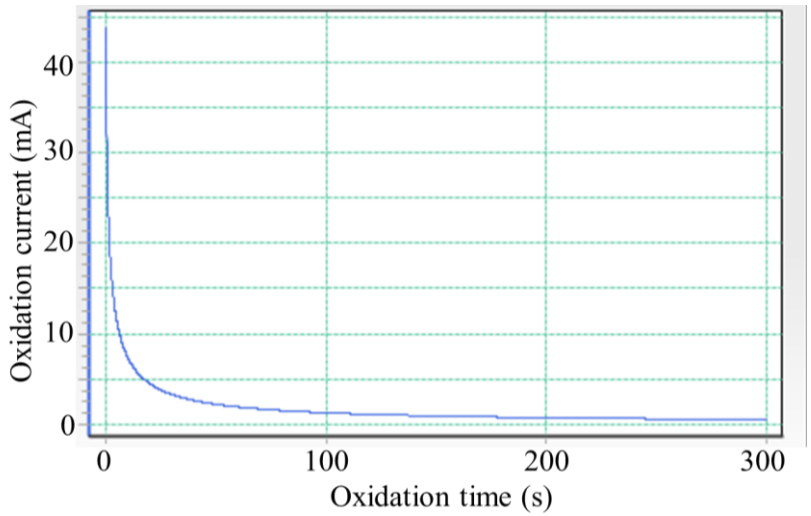

Figure 10. Relationship between oxidation current and oxidation time under the constant potential.

Therefore, based on the Eq. 8, Eq. 9, Eq. 10, Eq. 12, and Eq. 13, the numerical relationship between the oxidation depth *d*, the oxidation voltage *V*, the concentration of the electrolyte *c*, and the oxidation time *t* can be calculated, as shown in the Eq. 14.

$$d = \frac{2 \cdot \mu \cdot k \cdot M \cdot pK_{a1}^{\frac{1}{2}}}{8 \cdot 0.25 \cdot \pi \cdot r^2 \cdot D} \cdot V \cdot c^{\frac{1}{2}} \cdot t^{0.25} = \frac{\mu \cdot k \cdot M \cdot pK_{a1}^{\frac{1}{2}}}{\pi \cdot r^2 \cdot D} \cdot V \cdot c^{\frac{1}{2}} \cdot t^{\frac{1}{4}} \quad (14)$$

Taking the invariant part in Eq. 14 as a proportional coefficient *K*, the simplified expression of the Eq. 14 can be obtained, as shown in the Eq. 15.

$$d = K \cdot V \cdot c^{\frac{1}{2}} \cdot t^{\frac{1}{4}} \quad (15)$$

From the Eq. 15 it can be found that the oxidation depth *d* is proportional to the oxidation voltage *V*, half power of the concentration *c*, and quarter power of the oxidation time *t*. This is different from the traditional Deal-Grove model [22-24], in which the oxidation depth is proportional to half power of the oxidation time. The major reason for this phenomenon is that the Deal-Grove model is founded based on the diffusion principle in the thermal oxidation of Si, and the Eq. 15 is calculated according to the Ohm's law and electroanalysis in the anodic oxidation of RS-SiC. The generated oxide layer in the anodic oxidation of RS-SiC can not only resist the diffusion of oxidation radicle, but also increase the resistance of the oxidation circuit. Therefore, the relationship between the oxidation depth and the oxidation time in anodic oxidation of RS-SiC is different from that in thermal oxidation.

4.3 Calculation of the actual oxidation depth

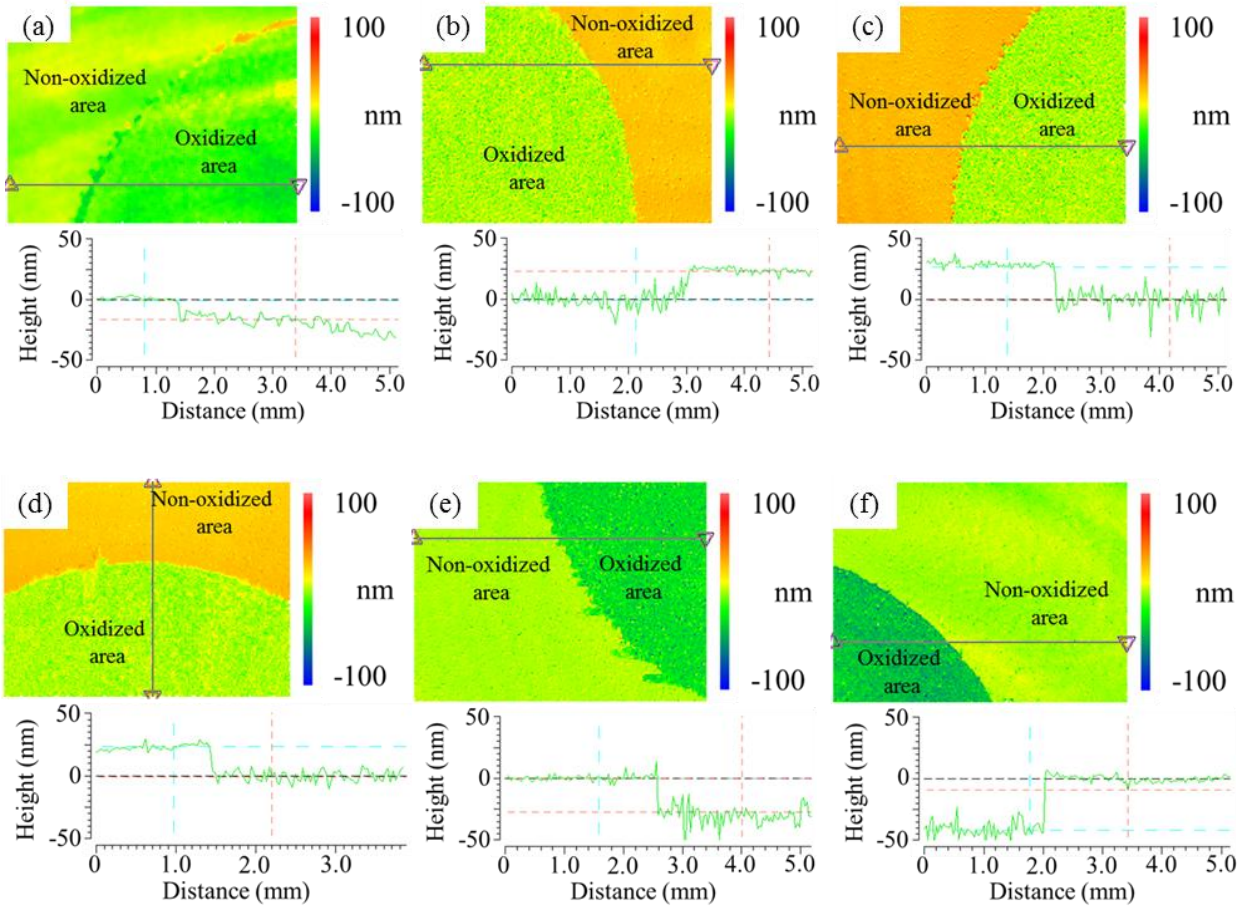

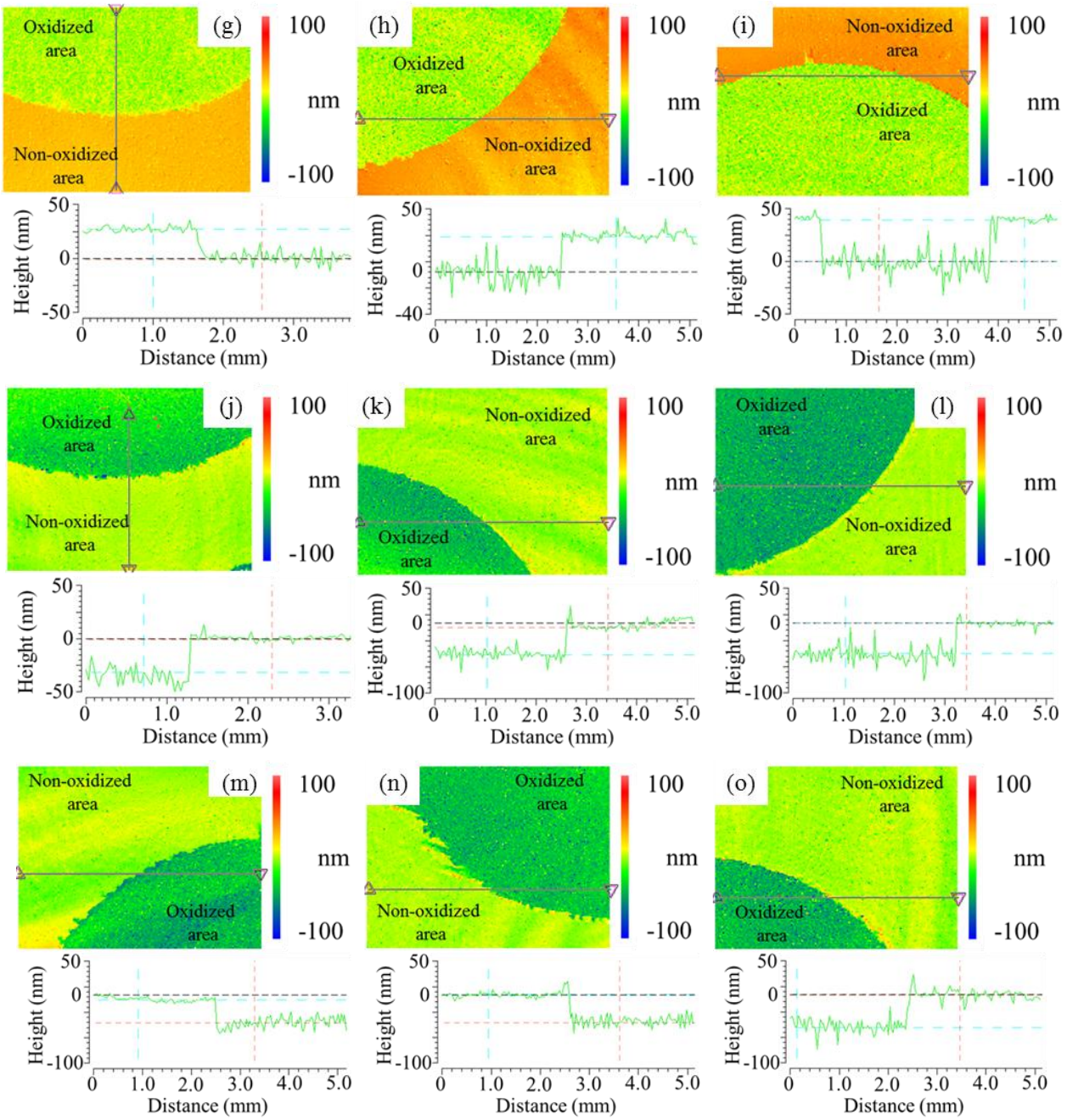

Figure 11. Calculations of the oxidation depth in anodic oxidation of RS-SiC under the constant potential for a certain oxidation time. (a) under 5V for 60s. (b) under 5V for 180s. (c) under 5V for 300s. (d) under 6V for 60s. (e) under 6V for 180s. (f) under 6V for 300s. (g) under 7V for 60s. (h) under 7V for 180s. (i) under 7V for 300s. (j) under 8V for 60s. (k) under 8V for 180s. (l) under 8V for 300s. (m) under 9V for 60s. (n) under 9V for 180s. (o) under 9V for 300s.

The actual oxidation depth in the constant potential mode is calculated by SWLI, which is aim to validate the relationship between oxidation depth and its influencing factors. The concentration of the electrolyte is 10wt%. The voltages are 5V, 6V, 7V, 8V, and 9V, respectively. The oxidation times are 60s, 180s, and 300s, respectively. After oxidation under a certain experimental condition, the oxidized RS-SiC sample is etched by hydrofluoric acid (HF) to remove the oxide. By comparing the

surfaces before and after HF etching, the oxidation depth can be calculated, as shown in Fig. 11(a) to Fig. 11(o). The anodic oxidation depth corresponding to a certain oxidation condition is summarized in Table 3.

Table 3. The summarized oxidation depth data corresponding to a certain oxidation condition.

Potential	Oxidation time	Concentration	Oxidation depth
5V	60s	10wt%	15.7nm
6V	60s	10wt%	24.1nm
7V	60s	10wt%	27.9nm
8V	60s	10wt%	30.6nm
9V	60s	10wt%	34.2nm
5V	180s	10wt%	23.9nm
6V	180s	10wt%	27.2nm
7V	180s	10wt%	33.8nm
8V	180s	10wt%	38.7nm
9V	180s	10wt%	42.4nm
5V	300s	10wt%	27.4nm
6V	300s	10wt%	32.8nm
7V	300s	10wt%	38.9nm
8V	300s	10wt%	43.7nm
9V	300s	10wt%	49.1nm

The oxidation depths and the oxidation parameters (*V*, *C*, *t*) in Table 3 for the oxidation times 60s and 180s are used to calculate the proportional coefficient *K* in the Eq. 15, as shown in Fig. 12. The *x*-coordinate in Fig. 12 is $V \cdot c^{\frac{1}{2}} \cdot t^{\frac{1}{4}}$, and the *y*-coordinate is the oxidation depth. It can be found that the linearity of the data in Fig. 12 is fine, and the calculated slope, which represents the proportional coefficient, is 0.418. Therefore, the relationship between the oxidation depth and its influencing factors can be obtained, as shown in Eq. 16.

$$d = 0.418 \cdot V \cdot c^{\frac{1}{2}} \cdot t^{\frac{1}{4}} \quad (16)$$

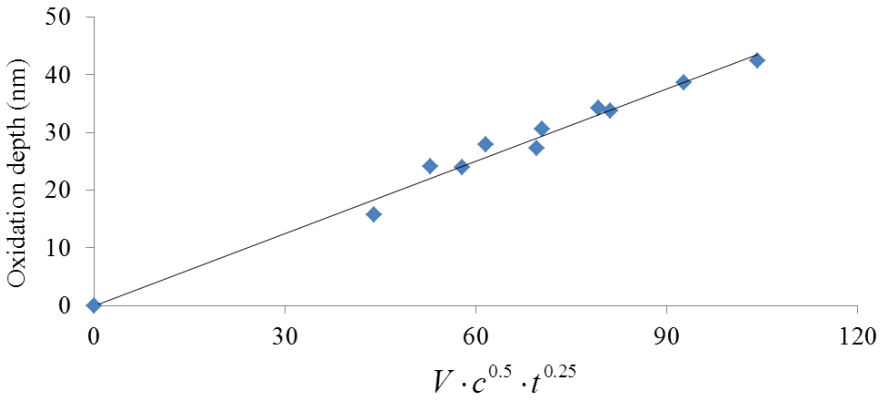

Figure 12. Calculation of the oxidation coefficient *K* based on the oxidation depth data.

Afterwards, the oxidation depth data in Table 3 when the oxidation time is 300s in Table 3 is used to verify the veracity of Eq. 16. Corresponding to the oxidation voltages of 5V, 6V, 7V, 8V, and 9V, the oxidation depths in Table 3 when oxidation time is 300s are 27.4nm, 32.8nm, 38.9nm, 43.7nm, and 49.1nm. The calculated oxidation depths based on Eq. 16 are 27.5nm, 33.0nm, 38.5nm, 44.1nm, and 49.6nm for oxidation voltages from 5V to 9V at the interval of 1V. It can be found that the fractional error between experimental data and theoretical data is smaller than 1%. Thus, the oxidation depth in anodic oxidation of RS-SiC by H_3PO_4 under the constant potential can be accurately controlled by adjusting the oxidation voltage, the concentration of the electrolyte, and the oxidation time, which can promote the application of anodically oxidation-assisted polishing of RS-SiC.

5. CONCLUSIONS

Oxidation characteristic and machining performance in anodically oxidation-assisted polishing of RS-SiC is studied in this research. The following conclusions are obtained:

(a) Relative to other technologies for machining RS-SiC, such as the diamond lapping [11, 13], plasma chemical vaporization machining (PCVM) [14], single point diamond turning (SPDT) [25], electrolytic in process dressing (ELID) grinding [26], and electric discharge milling [27], anodically oxidation-assisted polishing can obtain an ultrasmooth surface with roughness 8.520nm. Meanwhile, in the simultaneous anodically oxidation-assisted polishing of RS-SiC, the theoretical MRR can reach the level of μm/min, which is a remarkable improvement in machining RS-SiC ceramic.

(b) The oxidation characters and oxide morphologies under the two potential modes are compared by the SEM observation and SWLI measurement. There are protuberances and cracks on the oxidized RS-SiC samples in the two modes, and the anodic oxidation of RS-SiC under the constant potential can obtain a relative smooth morphology. Both the oxidized surfaces in the two modes are destroyed, and the surface roughness rms of the oxidized sample under the constant potential is 148.095nm, which is slightly better than that obtained in the HFSW potential mode. The results of qualitative investigation and quantitative analysis prove that anodic oxidation of RS-SiC by H_3PO_4 under the constant potential is propitious to obtain better surface quality with the assistant of abrasive polishing.

(c) The validation of machining performance of the oxide layers show that after abrasive polishing of the oxidized RS-SiC sample obtained in the constant potential mode, the surface roughness rms is 8.520nm, which is obviously better than that obtained under the HFSW potential (52.771nm). The results indicate that the anodically oxidation-assisted polishing, which includes anodic oxidation of RS-SiC by H_3PO_4 under the constant potential and abrasive polishing of oxide layer by CeO_2 slurry, can be considered as a practical method for the efficient machining of RS-SiC substrates.

(d) The relationship between the oxidation depth and its influencing factors in the anodic oxidation of RS-SiC under the constant potential are investigated based on the Ohm's law and the electroanalysis. The results of the theoretical analysis show that the oxidation depth is proportional to

the oxidation voltage, half power of concentration of the electrolyte, and quarter power of oxidation time.

(e) The actual oxidation depths obtained in certain experimental conditions are calculated by comparing the surface morphologies before and after HF etching of the oxidized RS-SiC samples. Based on the anodic oxidation depth data, the numerical relationship between the oxidation depth and its influencing factors is obtained through data fitting. The fractional error between experimental data and theoretical data is smaller than 1%. Thus, the oxidation depth in the anodic oxidation of RS-SiC by H_3PO_4 under the constant potential can be accurately controlled by adjusting the oxidation voltage, concentration of the electrolyte, and the oxidation time, which can promote the application of anodically oxidation-assisted polishing in machining RS-SiC.

ACKNOWLEDGEMENT
This work was supported by a grant from National Natural Science Foundation of China (Grant No. 51505498) and a grant from Natural Science Foundation of Jiangsu Province (Grant No. BK20150714). The authors also express their gratitude to the staffs and students of the Research Center for Ultra-precision Science and Technology of Osaka University.

References

1. Z.R. Huang, G.L. Liu, X.J. Liu, Z.M. Chen, and D.L. Jiang, *Proc. of SPIE*, 8335 (2012) 83351R.
2. S.Q. Ding, S.M. Zhu, Y.P. Zeng, and D.L. Jiang, *J. Eur. Ceram. Soc*., 27 (2007) 2095.
3. S.W. Pang, T. Tamamura, M. Nakao, A. Ozawa, and H. Masuda, *J. Vac. Sci. Technol*. B, 16(1998) 1145.
4. A. Sayano, C. Sutoh, S. Suyama, Y. Itoh, and S. Nakagawa, *J. Nucl. Mater*., 271–272(1999) 467.
5. S.P. Lee, Y.S. Shin, D.S. Bae, B.H. Min, J.S. Park, and A. Kohyama, *Fusion Eng. Des*., 81(2006) 963.
6. S. Suyama, T. Kameda, and Y. Itoh, *Diamond Related Materials*, 12 (2003) 1201.
7. S. Suyama, Y. Itoh, K. Tsuno, and K. Ohno, *Proc. SPIE*, 5868 (2005) 58680E.
8. H. Zhu, X.L. Liu, D.Y. Yan, and P. Ma, *Proc. of SPIE*, 8194 (2011) 81942A.
9. R.J. Ji, Y.H. Liu, Y.Z. Zhang, and F. Wang, *Int. Journal of Refractory Metals and Hard Materials*, 29 (2011) 117.
10. H.B. Cheng, Y.P. Feng, L.Q. Ren, S. To, and Y.T. Wang, *J. Mater. Process. Technol*., 209 (2009) 4563.
11. H.Y. Tam, H.B. Cheng, and Y.W. Wang, *J. Mater. Process. Technol*., 192-193 (2007) 276.
12. Z.Y. Zhang, J.W. Yan, and T. Kuriyagawa, *Int. J. Adv. Manuf. Technol*., 57 (2011) 117.
13. J.W. Yan, Z.Y. Zhang, and T. Kuriyagawa, *Int. J. Mach. Tools Manuf*., 49 (2009) 366.
14. K. Yamamura, Y. Yamamoto, and H. Deng, *Procedia* CIRP, 3 (2012) 335.
15. X.M. Shen, Y.F. Dai, H. Deng, C.L. Guan, and K. Yamamura, *Opt. Express*, 21 (2013) 14780.
16. X.M. Shen, Y.F. Dai, H. Deng, C.L. Guan, and K. Yamamura, *Opt. Express*, 21 (2013) 26123.
17. X.M. Shen, Q.Z. Tu, H. Deng, G.L. Jiang, and K. Yamamura, *Optical Engineering*. 54(2015): 055106.
18. W.S. Woon, S.D. Hutagalung, and K.Y. Cheong, *Thin Solid Films*, 517 (2009) 2808.
19. K. Yamauchi, H. Mimura, K. Inagaki, and Y. Mori, *Rev. Sci. Instrum*., 73 (2002) 4028–4033.
20. F.H. Zhang, X.Z. Song, Y. Zhang, and D.R. Luan, *J. Micromech. Microeng*., 19 (2009) 054009.
21. H. Deng, M. Ueda, and K. Yamamura, *Key Engineering Materials*, 516 (2012) 186.
22. B.E. Deal, and A.S. Grove, *J. Appl. Phys*., 36(1965) 3770.

23. Y. Song, S. Dhar, L.C. Feldman, G. Chung, and J.R. Williams, *J. Appl. Phys*., 95 (2004) 4953.
24. Z. Zheng, R.E. Tressler, and K.E. Spear, *J. Electrochem. Soc*., 3 (1990) 854.
25. S. Goel, X.C. Luo, and R.L. Reuben, *Computational Materials Science*, 51 (2011) 402.
26. H. Ohmori, Y. Dai, and W. Lin, *Key Engineering Materials*, 238 (2003) 65.
27. P.J. Liew, J. Yan, and T. Kuriyagawa, *Journal of Materials Processing Technology*, 213 (2013) 1076.